Obtaining Intense Attosecond Pulses in the Far Field from Relativistic Laser-Plasma Interactions

Y. Zhang,[1] C. L. Zhong,[1] S. P. Zhu,[2] X. T. He,[1,2] M. Zepf,[3] and B. Qiao[1,*]

[1] *Center for Applied Physics and Technology, HEDPS, and SKLNPT, School of Physics, Peking University, Beijing 100871, China*

[2] *Institute of Applied Physics and Computational Mathematics, Beijing 100094, China*

[3] *Helmholtz Institute Jena, 07743 Jena, Germany*

(Received 30 September 2020; revised 27 January 2021; accepted 10 August 2021; published 24 August 2021)

In this paper, we show that the Gouy phase shift plays a key role in the far-field waveform evolution of the reflected harmonic radiations from plasma surfaces driven by a relativistic Gaussian laser. With a proper adjustment of laser focal position away from the plasma surface, the inherent separations between the peaks of different harmonic carrier waves as well as the fundamental wave due to different wavelengths can be cleared away when they propagate from near to far field, since they experience the same Gouy phase shift of $\pi/2$. Using this method, intense attosecond pulses can be obtained in the far field with no need of any spectral filters. Three-dimensional particle-in-cell simulations show that far-field attosecond pulses with intensity of 4×10^{15} W/cm^2 (2.56×10^{17} W/sr; 65 times increase) and duration of 76 as (50% decrease) can be obtained by lasers at intensities of 10^{21} W/cm^2. Such brilliant pulses with fully reserved spectra significantly benefit applications in attosecond science.

DOI: 10.1103/PhysRevApplied.16.024042

I. INTRODUCTION

Attosecond light pulses provide insights into electron dynamics in atoms, molecules, and condensed matter [1–4], enabling highly time-resolved measurement and control of ultrafast dynamics in many applications [5]. Forming attosecond pulses requires a broad bandwidth of harmonics, which can be generated in interactions between lasers and matter including gases [6], crystals [7], and plasmas [8–12]. Due to there being no limitation on the drive laser intensity, relativistic high-order harmonic generation (RHHG) in overdense plasmas [13–16] is regarded as the most promising route to obtaining intense attosecond pulses at large photon energies and high brilliances.

In RHHG, high harmonics are produced by reflections of laser fields from a plasma mirror (PM) when the PM transverse current density changes the sign and longitudinal velocity approaches the maximum [17], which indicates all harmonic carrier waves including the fundamental wave have the same zero points (initial phase $\phi_0 = 0$) [18]. However, due to different wavelengths, the peaks of different harmonic waves ($\phi_0 = \pi/2$) are separated, with a maximum distance of approximately $\lambda_L/4$, where λ_L is the laser wavelength. Therefore, generally a high-pass spectral filter [19] is needed to obtain pulses with durations at attosecond scales, leading to rather low intensity and conversion efficiency [20,21], because the harmonic spectrum has a fast-decaying scaling of intensity I_n on the harmonic order n as $I_n \propto n^{-q}$ ($q \geq 4/3$) [16].

In addition, in RHHG the laser exerts such a high pressure on plasma surfaces that any spatial variation of laser intensity induces significant deformation of the PM—typically becoming curved [22] for Gaussian lasers. Influences of the optically curved PM on spatial [22–26] and spectral [27] properties of reflected pulses have been studied. However, another key effect, the Gouy phase shift $\Delta\phi_G$ [28,29], an extra phase change experienced by the focused harmonic waves during propagation, on the reflected pulse in far field has barely been investigated.

In this paper, through theoretical derivations and three-dimensional (3D) particle-in-cell (PIC) simulations, we show that the Gouy phase shift plays a key role in far-field waveform evolution of the reflected harmonics in RHHG. It is found that, when the laser focal position is adjusted to be away from target surfaces at an appropriate distance $x_f = (4\pi L/\lambda_L)x_R$, where $x_R = \pi w_L^2/\lambda_L$ is the Rayleigh length of the incident laser with focal waist w_L and L is the preplasma length scale, all harmonic waves including the fundamental frequency experience the same Gouy phase shift of $\Delta\phi_G = \pi/2$ when propagating from near to far field and their locked phases change from zero

*Corresponding author. bqiao@pku.edu.cn

to $\pi/2$. As a result, the inherent separations for the peaks of different harmonic waves are cleared away. Based on this, a scheme for production of intense attosecond pulses in far field with no need of spectral filters is proposed, which is much more practical than those using artificially super-Gaussian lasers or specially designed targets [27,30]. Due to the millijoule-level energy and fully reserved reflection spectra of the generated attosecond pulses, our scheme has great potential in realizing and developing attosecond-pump-attosecond-probe experiments [1,2].

II. THEORETICAL ANALYSIS

As shown schematically in Fig. 1(a), the electric field of the reflected pulse (RP) evolves significantly from near (green) to far (red) field from an optically curved PM driven by Gaussian lasers due to the Gouy phase shift. The Gouy phase shift $\Delta\phi_{Gn}$ that the nth-order harmonic wave including $n = 1$ experiences from near to far field is composed of two parts: one from the PM surface to its focal plane with distance x_{fn} and the other from its focal plane to the far field with distance $x_{\rm far}/x_{Rn} \approx \infty$, where $x_{Rn} = n\pi w_{fn}^2/\lambda_L$ is its Rayleigh length and w_{fn} is its waist at the focal plane. Assuming all harmonic waves also have a Gaussian spatial distribution, according to Ref. [29], we get that

$$\Delta\phi_{Gn} = -\arctan(x_{fn}/x_{Rn}) + \pi/2, \tag{1}$$

where $x_{fn} < 0$ if wave fronts of harmonics on PMs are concave and $x_{fn} \geq 0$ otherwise. We define the waist of harmonic waves on the PM surface as $w_{sn} = \beta_n w_s$ [23], where the coefficient $\beta_n \leq 1$ is almost independent of laser intensities and preplasma length scales and $w_s = w_L\sqrt{1 + (x_f/x_R)^2}$ is the incident laser waist on the PM surface. For $n = 1$, $w_{s1} = \beta_1 w_s = w_s$ ($\beta_1 = 1$) is satisfied for that the reflected fundamental laser wave has the same waist as the incident wave. Similarly, we have $w_{sn} = w_{fn}\sqrt{1 + (x_{fn}/x_{Rn})^2}$. After derivations, we obtain that the focal position x_{fn} satisfies the relation $x_{fn}^2/x_{Rn}^2 = n\beta_n^2(1 + x_f^2/x_R^2)(x_R/x_{Rn}) - 1$.

Further, for all reflected harmonics, the curvature radii should be the same as $R_r = x_{fn} + x_{Rn}^2/x_{fn}$, while for the normally incident laser $R_i = x_f + x_R^2/x_f$. Assuming the target has an exponential density profile with length scale L, the PM is bent as a parabolic mirror with focal length $f_p \approx w_s^2/4L = x_R[1 + (x_f/x_R)^2]/b$ ($b = 4\pi L/\lambda_L$) [22], which depends on the distribution of the incident laser intensity, instead of the intensity itself. For a parabolic mirror, we have $1/R_i - 1/R_r = 1/f_p$ [31]. Substituting for R_r and R_i,

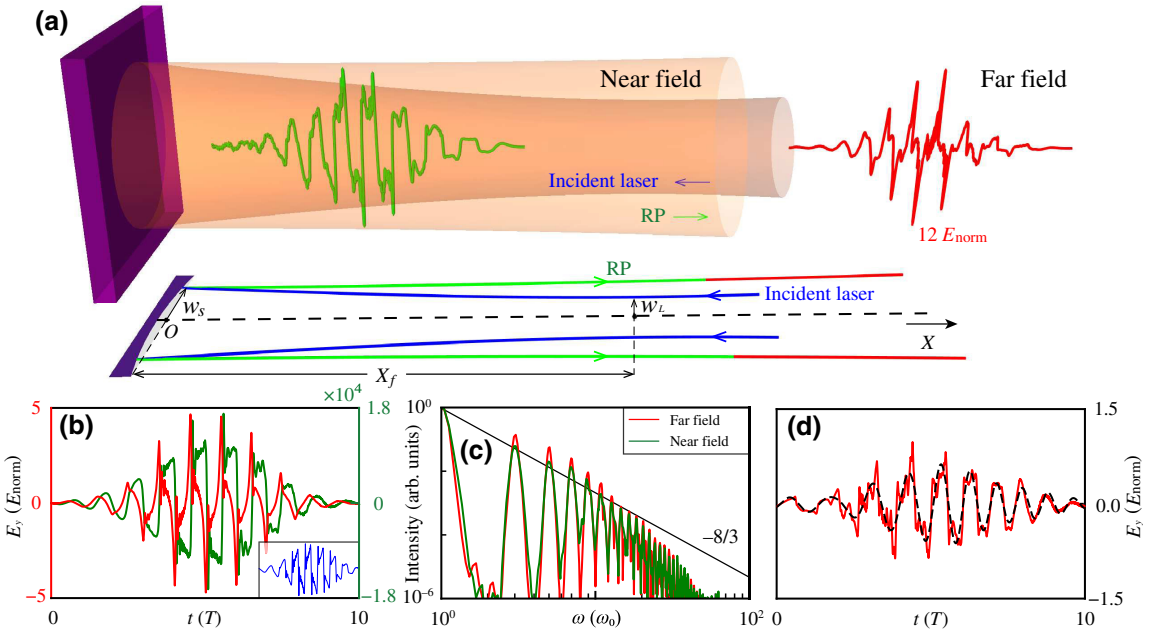

FIG. 1. (a) Schematic for electric field evolution from the near to far field of the RP (green arrow) in RHHG, where a Gaussian laser (blue arrow) is incident on a solid target (gray block) and an optically curved PM (purple block) is formed. The temporal profiles of E_y on the x axis of the RP in the near (green) and far (red) fields, obtained from 3D PIC simulations with laser focal position $x_f = bx_R$ and preplasma length scale $L = 0.2\lambda_L$, are plotted. (b) Temporal profiles of E_y on the x axis of the RP in the near (green) and far (red) fields for the case $x_f = 0$ and $L = 0$, where the inset (blue) shows E_y in the far field after shifting back a phase $\pi/2$. (c) The harmonic spectra for the cases in (b). (d) Temporal profile of E_y (red) of the far-field RP in the simulation of (a) but for $x_f = 0$, where the black dashed line shows the fundamental component. Note that all values of E_y are normalized by the maximum E_y (red) in (d) and other parameters are described in the text.

we obtain that x_{fn} also satisfies the relation $x_{fn} + x_{Rn}^2/x_{fn} = (x_f^2 + x_R^2)/(x_f - bx_R)$.

From the above two relationships, we can write two more useful equations as

$$\frac{x_{fn}}{x_{Rn}} = n\beta_n^2\left(\frac{x_f}{x_R} - b\right), \tag{2}$$

$$x_{fn}^2 + x_{Rn}^2 = \frac{\left(x_f^2 + x_R^2\right)^2}{\left(n^2\beta_n^4\right)^{-1}x_R^2 + \left(x_f - bx_R\right)^2}. \tag{3}$$

Substituting Eq. (2) into Eq. (1) as well as the expression of w_{fn}, we obtain the Gouy phase shift and the beam waist of the nth-order harmonic wave from near to far field as, respectively,

$$\Delta\phi_{Gn} = \arctan\left[n\beta_n^2\left(b - \frac{x_f}{x_R}\right)\right] + \frac{\pi}{2}, \tag{4}$$

$$w_{fn} = \beta_n w_L\sqrt{\frac{1 + \left(x_f/x_R\right)^2}{1 + n^2\beta_n^4\left(b - x_f/x_R\right)^2}}. \tag{5}$$

From Eq. (4), if the laser focal position is adjusted as $x_f = bx_R = (4\pi L/\lambda_L)x_R$, all harmonic waves experience the same $\Delta\phi_{Gn} = \pi/2$, resulting in a change of their locked phase from $\phi = 0$ (zero points) to $\pi/2$ (peak points) when propagating from near to far field. This means that the peaks of all harmonic waves (including the fundamental one) overlap in the far field, naturally forming a sharp peak in RPs for attosecond production. In other words, we can get intense attosecond pulses in the far field with no need of spectral filters, where the intensity is greatly increased, comparing with that if $x_f = 0$ is chosen and low-order harmonics have to be filtered. Further, from Eq. (5) we see that for $x_f = bx_R$, all harmonic waves have almost the same beam waist $w_{fn} = \beta_n w_L\sqrt{1 + (x_f/x_R)^2}$, i.e., having small divergence angles when propagating from focal plane to far field, which also helps in increasing the attosecond intensity in far field. For $x_f = 0$, though the harmonic intensity increases at the focal plane as $w_{fn} \sim w_L/n\beta_n b$ [32], it decreases significantly in far field.

Next, we analyze the harmonic spectrum evolution from near field I_n^{near} to far field I_n^{far}. Considering the focusing effect of a parabolic PM, we have

$$I_n^{\text{far}} = I_n^{\text{near}}\frac{1 + (x_{fn}/x_{Rn})^2}{1 + (x_{\text{far}}/x_{Rn})^2}. \tag{6}$$

Due to the far-field condition $x_{\text{far}}/x_{Rn} \approx \infty$, the far-field harmonic spectrum is then $I_n^{\text{far}}/I_1^{\text{far}} \approx (I_n^{\text{near}}/I_1^{\text{near}})[(x_{Rn}^2 + x_{fn}^2)/(x_{R1}^2 + x_{f1}^2)] = (I_n^{\text{near}}/I_1^{\text{near}})\{n^2[(b - x_f/x_R)^2 + 1])/(n^2(b - x_f/x_R)^2 + \beta_n^{-4})\}$, where $\beta_1 = 1$ is taken and Eq. (3) is used. If assuming $I_n^{\text{near}}/I_1^{\text{near}} \propto n^{-8/3}$ such as for a relativistically oscillating mirror (ROM) mechanism [14,22], we obtain

$$I_n^{\text{far}}/I_1^{\text{far}} \propto n^{-8/3} \times \frac{n^2[(b - x_f/x_R)^2 + 1]}{n^2(b - x_f/x_R)^2 + \beta_n^{-4}}. \tag{7}$$

We see that if $x_f = bx_R$, the scaling of the far-field harmonic spectrum is improved as much slower as $I_n^{\text{far}}/I_1^{\text{far}} \propto n^{-2/3}$. This is because, when a planarlike PM is formed ($x_f = bx_R$), the divergence angles of the reflected harmonics θ_n depend inversely on the harmonic orders n, i.e., $\theta_n = \lambda_L/n\pi w_{fn} \propto (n\beta_n)^{-1}$ [from Eq. (5)].

Finally, the improvement of far-field intensity of reflected harmonics when $x_f = bx_R$ can be briefly evaluated through comparing with the unoptimized situation ($x_f = 0$). Utilizing Eqs. (3) and (6) and the far-field condition with $I_n^{\text{near}} = \eta_n I_0\left[1 + \left(x_f/x_R\right)^2\right]^{-1}$ assumed, we have

$$\frac{I_n^{\text{far},bx_R}}{I_n^{\text{far},0}} = (1 + b^2)\left[(\beta_n^0)^{-4} + n^2b^2\right]\left(\beta_n^{bx_R}\right)^4\frac{\eta_n^{bx_R}}{\eta_n^0}, \tag{8}$$

where η_n and superscripts bx_R and 0 represent the generation efficiency of nth-order harmonics and values of x_f, respectively. Clearly, as usually $n^2b^2 \gg (\beta_n^0)^{-4}$ and $\eta_n^{bx_R} \sim \eta_n^0$ for intense incident lasers [33], $I_n^{\text{far},bx_R}/I_n^{\text{far},0} \sim n^2b^2(1 + b^2)(\beta_n^{bx_R})^4$, which can be much greater than 1 for high-order harmonics.

III. SIMULATION RESULTS

To verify the theory, 3D PIC simulations with code EPOCH [34] are carried out. A parallel time-domain near-to-far-field transformation [35,36] module based on the Kirchhoff diffraction theory [37] is developed to self-consistently calculate the far-field waveform evolution. Figure 1(a) shows the simulation setup. The target is composed of a thin foil with density $n_0 = 100n_c$ ($n_c = m_e\omega_L^2/4\pi e^2$) and thickness $0.5\lambda_L$ from $x = 0$ and a preplasma with exponential density distribution $n(x) = n_0\exp[-(x - 0.5\lambda_L)/L]$. A laser with intensity 1.93×10^{21} W/cm^2 and $\lambda_L = 800$ nm (amplitude $a_0 = 30$) is incident from the right-hand boundary. The laser has Gaussian distributions in both space and time with duration $\tau_L = 8$ fs $\sim 3T$ and focal waist $w_L = 2$ μm, where $T = \lambda_L/c$ is the laser period. The simulation box ($x \times y \times z$) is $7 \times 28 \times 28$ λ_L^3 containing $2100 \times 1400 \times 1400$ cells. The particle number per cell is 4 for electrons and 2 for ions. Ions are immobile to save on computational resources, while the influence of their movement is discussed in the Appendix.

Figure 1(b) shows the temporal profile of the reflected field E_y on the x axis when the laser focal position is at the target surface and no preplasma exists, i.e., $x_f = 0$ and $L = 0$. We see that the far-field waveform (red) is modulated significantly compared with the near-field one (green)

due to the Gouy phase shift. Since all harmonic waves experience the same $\Delta\phi_{Gn} = \pi/2$ [Eq. (4)] and the harmonic spectra in near and far fields have the same scaling $-8/3$ [Fig. 1(c)], the far-field waveform can be transformed back to the near-field one by just shifting back a phase $\pi/2$; see the blue line in the inset of Fig. 1(b) in comparison with the green line.

Generally, the preplasma length scale is $L \neq 0$, and according to Eq. (4), we adjust the laser focal position at $x_f = bx_R = (4\pi L/\lambda_L)x_R$ to obtain intense attosecond pulses in the far field. The red line in Fig. 1(a) shows reflected E_y when $x_f = bx_R \approx 49.4\lambda_L$ and $L = 0.2\lambda_L$. We see that intense attosecond pulses are naturally obtained, where all harmonics and the fundamental frequency are included with no need of filters. On the contrary, if still choosing $x_f = 0$, Fig. 1(d) shows the RPs (red) have much wider durations with peaks that are not obvious, because the peaks of the fundamental (black dashed line) and harmonic waves (red) are separated. Generally, it is required to filter the fundamental and low-order harmonics so that the RP durations after filtering are within attosecond scales, leading to significant decreases of their intensities. The detailed dynamics can also be seen from Fig. 2(a), which shows E_y for high harmonics ($n > 1$) and the fundamental frequency around the peak laser intensity cycle.

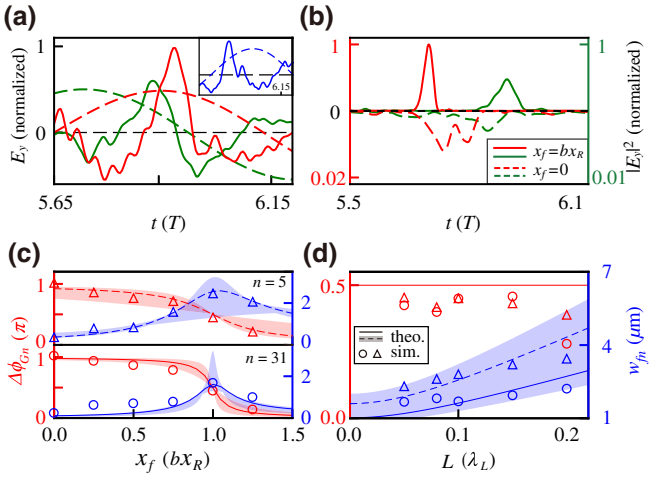

FIG. 2. (a) On-axis far-field electric field E_y of high harmonics (solid, $n > 1$) and the fundamental frequency (dashed) in RP in 3D simulations, where $x_f = 0$ (green, for which the value is magnified by 8 times) and $x_f = bx_R \approx 49.4\lambda_L$ (red) are taken, respectively. The inset shows the near-field results. (b) On-axis far-field $|E_y|^2$ for $L = 0.1\lambda_L$ (red) and $0.2\lambda_L$ (green) when $x_f = bx_R$ (solid) and $x_f = 0$ (dashed). (c) Dependences of the Gouy phase shift $\Delta\phi_{Gn}$ and beam waist w_{fn} on x_f for the 5th-order (dashed when $\beta_5 = 0.8$, shading when $0.4 < \beta_5 < 1$) and 31st-order (solid when $\beta_{31} = 0.5$, shading when $0.4 < \beta_{31} < 1$) harmonics, where the curved lines are from Eqs. (4) and (5) and triangle and circle symbols represent simulation results. (d) Similar to (c), but for those depending on L, where $x_f = bx_R$.

In near field [inset of Fig. 2(a)], as expected [18], the harmonic and fundamental waves have almost the same zero points ($\phi_0 = 0$) while their peaks ($\phi_0 = \pi/2$) are separated (comparing the blue solid lines with dashed lines). This results in separation of their peaks in far field as well if $x_f = 0$ is still taken (green lines). However, by adjusting $x_f = bx_R$, the separation between their peaks can be almost cleared away in far field for $\Delta\phi_{Gn} = \pi/2$ (comparing the red solid lines and dashed lines).

The scheme works for a broad range of parameters. Figure 2(b) shows the RP intensity $|E_y|^2$ for $L = 0.1\lambda_L$ (red solid line) and $0.2\lambda_L$ (green solid line) around the peak laser intensity cycle. We see that by adjusting $x_f = bx_R$, for both cases an intense attosecond pulse is obtained with no need of spectral filters. Furthermore, since the optimum preplasma length scale of the ROM is approximately $\lambda_L/8$, $|E_y|^2$ for the case $L = 0.1\lambda_L$ is higher than for the case $L = 0.2\lambda_L$. However, if still choosing $x_f = 0$, the RPs (the dashed red and green lines) have much broader durations and lower intensities, where high-pass spectral filters are needed. Figures 2(c) and 2(d) show dependences of $\Delta\phi_{Gn}$ and w_{fn} for the 5th-order ($n = 5$) and 31st-order ($n = 31$) harmonic waves on x_f ($L = 0.1\lambda_L$) and L ($x_f = bx_R$), respectively. We see that the simulation results (triangle and circle symbols) agree well with the theoretical results (curved lines) from Eqs. (4) and (5). The slight differences for $n = 31$ in the range $x_f/bx_R \leq 0.5$ and $L/\lambda_L \geq 0.2$ are due to increased instabilities from tight harmonic refocusing and larger-scale preplasmas. Further, as expected, for $x_f = bx_R$ both waves achieve $\Delta\phi_{Gn} \approx \pi/2$. Simulations verify that the scheme also works at moderate intensities of approximately 10^{19} W/cm^2.

Figure 3(a) shows divergence angles θ_n of the harmonics in far field for $x_f = bx_R$ (red square) and $x_f = 0$ (blue square). We see that θ_n for the former case is smaller than for the latter case for all harmonics, i.e., having larger waist w_{fn} at the focal plane. This can be explained by Fig. 3(c) in that the RP has a planar wave front when $x_f = bx_R$, where the focusing effect of the curved PM is offset by the diverging wave front of the defocused laser, while the RP for $x_f = 0$ has a focusing wave front [Fig. 3(d)], leading to smaller w_{fn} but larger θ_n. Further, we see that for $x_f = bx_R$, the dependence of θ_n on n is consistent with the diffraction limit [38] $\theta_n = \theta_1/n$ [comparing the red square with red line in Fig. 3(a)], because all harmonics have almost the same $w_{fn} = \beta_n w_L\sqrt{1 + (x_f/x_R)^2}$ [Eq. (5)]. As shown in Fig. 3(b), such decreased θ_n also leads to great improvement of harmonic intensities in far field, although the laser intensity on the PM surface is lower due to defocusing. Specifically, the growth approaches 40 and 211 times for $n = 5$ and 31, respectively, close to the predictions of Eq. (8), which are 42 and 245 times. Here, $\beta_5^{bx_R} \approx 0.8$ and $\beta_{31}^{bx_R} \approx 0.5$ are used, as indicated in Fig. 2(c).

Figure 4(a) plots intensity distributions of the obtained attosecond pulses in far field at $x_{\text{far}} = 10^5\lambda_L$ for three

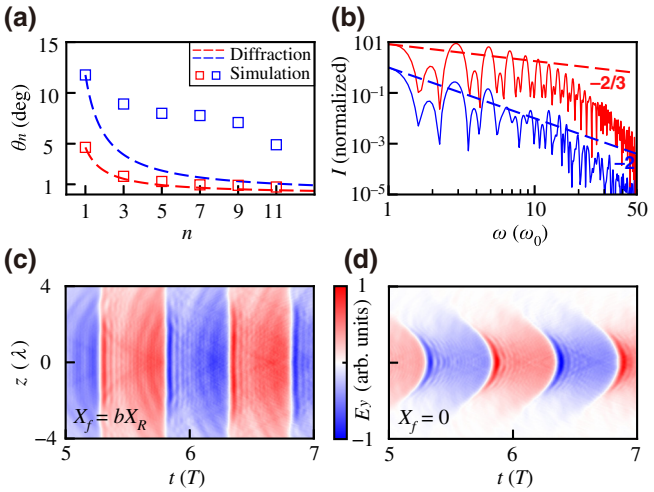

FIG. 3. (a) Divergence angles $\theta_n = \lambda_L/n\pi w_{fn}$ of the reflected harmonic waves in the far field varying with different n for the cases of $x_f = bx_R$ (red square) and $x_f = 0$ (blue square), where the dashed lines are calculated from the diffraction limit $\theta_n = \theta_1/n$. (b) The harmonic spectra on the x axis in the far field, where all intensities are normalized by the reflected fundamental one for $x_f = 0$. (c),(d) Spatial-temporal distributions of E_y on the t-z plane ($y = 0$) in near field for the cases of $x_f = bx_R$ and $x_f = 0$.

cases of $x_f = bx_R \approx 24.7\lambda_L$ and $L = 0.1\lambda_L$ (red), $x_f = 0$ and $L = 0.1\lambda_L$ (blue), and $x_f = 0$ and $L = 0$ (green). As expected, when adjusting $x_f = bx_R$, intense attosecond pulses with peak intensity of 4×10^{15} W/cm^2 (2.56×10^{17} W/sr) and duration of 76 as are obtained without any spectral filters, where the intensity is increased by 65 times

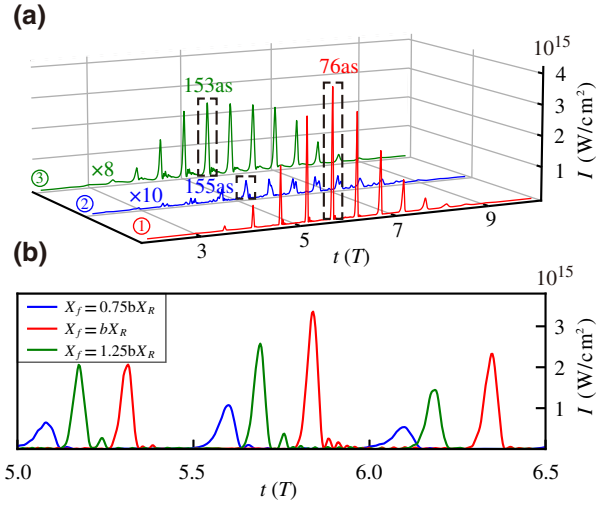

FIG. 4. (a) Intensity distributions of the obtained attosecond pulses in the far field at distance $x_{\rm far} = 10^5\lambda_L$ for three cases of $x_f = bx_R \approx 24.7\lambda_L$ and $L = 0.1\lambda_L$ (red), $x_f = 0$ and $L = 0.1\lambda_L$ (blue), and $x_f = 0$ and $L = 0$ (green). (b) Intensity distribution $|E_y|^2$ of the RP on the x axis for three cycles around the peak laser intensity when $x_f = 0.75bx_R$, bx_R, and $1.25bx_R$.

and the duration is decreased by half compared with the case without adjustment. The scaling of the harmonic spectra is improved to be much slower as $n^{-2/3}$ [see Fig. 3(b)]. Besides, as the whole reflection spectra are reserved, the energy of the attosecond pulses is at the level of millijoules. Furthermore, if the laser focal position deviates slightly from the optimal value, such as $x_f = 0.75bx_R$ and $1.25bx_R$, as shown in Fig. 4(b), we can still get intense attosecond pulses without filters at slightly lower intensities. This corresponds to an allowable error of approximately 10 μm for target orientation, much larger than the currently achievable precision (approximately 1 μm) in experiments [39].

IV. SUMMARY AND DISCUSSION

In summary, we show that the Gouy phase shift plays a key role in far-field waveform evolution of the reflected pulse in RHHG. With an appropriate adjustment of the laser focal position at $x_f = (4\pi L/\lambda_L)x_R$, intense attosecond pulses can be obtained in far field with no need of spectral filters. Note that, if the laser is obliquely incident with an angle α and ion motions are included, we just need to redefine the PM focal length as $f_p \approx w_s^2 h/4L\cos^2\alpha$ [22], where the coefficient h represents the influences of ion motion, and then our scheme still works by modifying $x_f = (4\pi L\cos\alpha/h\lambda_L)x_R$. Besides, our scheme also works for top-hat beams [40], which can be expressed as the superposition of Laguerre-Gauss (LG) beams with different modes. On the one hand, the final Gouy phase of the beam in far field is always $\pi/2$, independent of the order (p) of the LG modes, when considering both its initial phase $-p\pi$ and Gouy phase shift $(p + 1/2)\pi$ from focus to far field; on the other hand, the transverse intensity distribution of the focused top-hat beam, which is like an Airy pattern at the focus, evolves and eventually becomes just like that of a defocused Gaussian beam when it propagates and reaches the plasma surface [41].

It is worth noting that our scheme not only greatly simplifies the setting of experiments due to there being no requirements of filters, but also generates millijoule-level attosecond pulses naturally with whole spectra reserved. Such brilliant pulses benefit applications in attosecond science, especially real attosecond-pump-attosecond-probe experiments [1,2] that are limited by nanojoule-level attosecond pulses obtained typically from gaseous high-order harmonic generation [42,43]. Besides, attosecond pulses with intensity of the order of 10^{13}–10^{15} W/cm^2 can be used to study strong field interactions [44] including optical field ionization [45,46] and nonlinear cluster dynamics [47,48]. What is more, the reserved spectra ranging from near ultraviolet to vacuum ultraviolet ($\lesssim 30$ eV) provide avenues for researches in bound-electron dynamics [49,50], valence-shell phenomena [51], double ionization of helium atoms [52], and even control of chemical

reactions through selective excitation in molecules [53,54], which have been usually limited or forbidden in the past due to the introduction of high-pass filters.

ACKNOWLEDGMENTS

This work is supported by Science Challenge Project (No. TZ2018005); National Natural Science Foundation of China (Grants No. 11825502, No. 11921106, and No. 12075014); the Strategic Priority Research Program of Chinese Academy of Sciences (Grant No. XDA25050900); and the National Key R & D Program of China (Grant No. 2016YFA0401100). B.Q. acknowledges support from National Natural Science Funds for Distinguished Young Scholar (Grant No. 11825502). The simulations were carried out on the Tianhe-2 supercomputer at the National Supercomputer Center in Guangzhou.

APPENDIX: INFLUENCE OF ION MOVEMENT IN OUR SCHEME

As discussed in the main text, the influence of ion movement in our scheme is represented by coefficient h, which can be expressed as [22]

$$h = \frac{\epsilon + (1+\mu\epsilon)^2}{\epsilon + 2\mu\epsilon(1+\mu\epsilon)}, \tag{A1}$$

$$\epsilon = \frac{a_L(t)}{\pi L/\lambda_L(1-\sin\alpha)}, \tag{A2}$$

$$\mu = \frac{\omega_L(1-\sin\alpha)\Pi_0}{4}\int_{-\infty}^{t}\frac{a_L(t_0)}{a_L(t=t_{\max})}dt_0, \tag{A3}$$

$$\Pi_0 \equiv \sqrt{\frac{RZm_e\cos\alpha}{2AM_p}}, \tag{A4}$$

where R, Z, A, m_e, and M_p represent the plasma reflectivity coefficient for the laser, the average charge state, mass number of the ions, the electron mass, and the proton mass, respectively. Note that $t_{\max}$ represents the time when the laser amplitude a_L, which acts on PMs, reaches its peak value a_{peak}, i.e., $a_L(t=t_{\max}) = a_{\text{peak}}$.

Utilizing Eqs. (A1)–(A4), we calculate the value of h around $t_{\max}$ with different a_{peak} for $L = 0.1\lambda_L$ and $0.2\lambda_L$, where $R = 0.7$, $Z = 6$, $A = 12$, and $\alpha = 0$. And as shown in Fig. 5(a), h is always close to 1 and varies slowly in a rather large parameter range, including cases considered in our paper, which indicate that the influence of ion motion is negligible. Furthermore, as illustrated in Fig. 5(b), 3D simulations are carried out with mobile ions when $x_f = bx_R \approx 24.7\lambda_L$ and $L = 0.1\lambda_L$. Clearly, the on-axis intensity distributions of attosecond pulse trains obtained in the far field ($x_{\text{far}} = 10^5\lambda_L$) are almost the same, no matter whether ions are movable (red dashed) or immovable (black solid). Therefore, although the laser intensity used in RHHG is quite high, the influence of ion movement is negligible in our scheme and it is reasonable to set ions as immobile in PIC simulations.

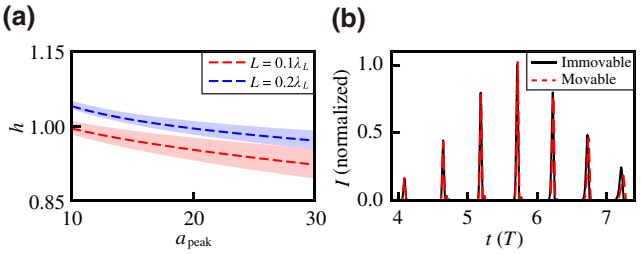

FIG. 5. (a) Dependences of the coefficient h on a_{peak} for $L = 0.1\lambda_L$ (red) and $0.2\lambda_L$ (blue) when $t = t_{\max}$ (dashed) as well as $|t - t_{\max}| \leq 0.5T$ (shading). (b) On-axis intensity distributions of the far-field attosecond pulses obtained from cases with movable (red dashed) or immovable (black solid) ions, where $x_{\text{far}} = 10^5\lambda_L$, $x_f = bx_R \approx 24.7\lambda_L$, and $L = 0.1\lambda_L$.

[1] F. Krausz and M. Ivanov, Attosecond physics, Rev. Mod. Phys. **81**, 163 (2009).
[2] F. Lépine, M. Y. Ivanov, and M. J. J. Vrakking, Attosecond molecular dynamics: Fact or fiction?, Nat. Photonics **8**, 195 (2014).
[3] Z. H. Chang, P. B. Corkum, and S. R. Leone, Attosecond optics and technology: Progress to date and future prospects [invited], J. Opt. Soc. Am. B: Opt. Phys. **33**, 1081 (2016).
[4] F. Krausz and M. I. Stockman, Attosecond metrology: From electron capture to future signal processing, Nat. Photonics **8**, 205 (2014).
[5] P. B. Corkum and F. Krausz, Attosecond science, Nat. Phys. **3**, 381 (2007).
[6] C. Winterfeldt, C. Spielmann, and G. Gerber, Colloquium: Optimal control of high-harmonic generation, Rev. Mod. Phys. **80**, 117 (2008).
[7] S. Ghimire, A. D. DiChiara, E. Sistrunk, P. Agostini, L. F. DiMauro, and D. A. Reis, Observation of high-order harmonic generation in a bulk crystal, Nat. Phys. **7**, 138 (2011).
[8] U. Teubner and P. Gibbon, High-order harmonics from laser-irradiated plasma surfaces, Rev. Mod. Phys. **81**, 445 (2009).
[9] C. Thaury, F. Quéré, J. P. Geindre, A. Levy, T. Ceccotti, P. Monot, M. Bougeard, F. Réau, P. d'Oliveira, and P. Audebert *et al.*, Plasma mirrors for ultrahigh-intensity optics, Nat. Phys. **3**, 424 (2007).
[10] B. Dromey, S. Rykovanov, M. Yeung, R. Hörlein, D. Jung, D. Gautier, T. Dzelzainis, D. Kiefer, S. Palaniyppan, and R. Shah, Coherent synchrotron emission from electron nanobunches formed in relativistic laser–plasma interactions, Nat. Phys. **8**, 804 (2012).
[11] X. Xu, Y. Zhang, H. Zhang, H. Lu, W. Zhou, C. Zhou, B. Dromey, S. Zhu, M. Zepf, and X. He *et al.*, Production of 100-tw single attosecond *x*-ray pulse, Optica **7**, 355 (2020).
[12] Y. X. Zhang, S. Rykovanov, M. Y. Shi, C. L. Zhong, X. T. He, B. Qiao, and M. Zepf, Giant Isolated Attosecond

Pulses from Two-Color Laser-Plasma Interactions, Phys. Rev. Lett. **124**, 114802 (2020).
[13] R. Lichters, J. MeyerterVehn, and A. Pukhov, Short-pulse laser harmonics from oscillating plasma surfaces driven at relativistic intensity, Phys. Plasmas **3**, 3425 (1996).
[14] T. Baeva, S. Gordienko, and A. Pukhov, Theory of high-order harmonic generation in relativistic laser interaction with overdense plasma, Phys. Rev. E **74**, 046404 (2006).
[15] D. an der Brügge and A. Pukhov, Enhanced relativistic harmonics by electron nanobunching, Phys. Plasmas **17**, 033110 (2010).
[16] M. R. Edwards and J. M. Mikhailova, The *x*-ray emission effectiveness of plasma mirrors: Reexamining power-law scaling for relativistic high-order harmonic generation, Sci. Rep. **10**, 5154 (2020).
[17] J. M. Mikhailova, M. V. Fedorov, N. Karpowicz, P. Gibbon, V. T. Platonenko, A. M. Zheltikov, and F. Krausz, Isolated Attosecond Pulses from Laser-Driven Synchrotron Radiation, Phys. Rev. Lett. **109**, 245005 (2012).
[18] S. Tang and N. Kumar, Ultraintense attosecond pulse emission from relativistic laser-plasma interaction, Plasma Phys. Control. Fusion **61**, 025013 (2019).
[19] G. D. Tsakiris, K. Eidmann, J. Meyer-ter-Vehn, and F. Krausz, Route to intense single attosecond pulses, New J. Phys. **8**, 19 (2006).
[20] B. Dromey, M. Zepf, A. Gopal, K. Lancaster, M. S. Wei, K. Krushelnick, M. Tatarakis, N. Vakakis, S. Moustaizis, and R. Kodama *et al.*, High harmonic generation in the relativistic limit, Nat. Phys. **2**, 456 (2006).
[21] C. Rödel, D. an der Brügge, J. Bierbach, M. Yeung, T. Hahn, B. Dromey, S. Herzer, S. Fuchs, A. G. Pour, and E. Eckner *et al.*, Harmonic Generation from Relativistic Plasma Surfaces in Ultrasteep Plasma Density Gradients, Phys. Rev. Lett. **109**, 125002 (2012).
[22] H. Vincenti, S. Monchocé, S. Kahaly, G. Bonnaud, P. Martin, and F. Quéré, Optical properties of relativistic plasma mirrors, Nat. Commun. **5**, 3403 (2014).
[23] F. Quéré, C. Thaury, J.-P. Geindre, G. Bonnaud, P. Monot, and P. Martin, Phase Properties of Laser High-Order Harmonics Generated on Plasma Mirrors, Phys. Rev. Lett. **100**, 095004 (2008).
[24] M. Geissler, S. Rykovanov, J. Schreiber, J. Meyer-Ter-Vehn, and G. D. Tsakiris, 3d simulations of surface harmonic generation with few-cycle laser pulses, New J. Phys. **9**, 218 (2007).
[25] M. Yeung, B. Dromey, D. Adams, S. Cousens, R. Hörlein, Y. Nomura, G. D. Tsakiris, and M. Zepf, Beaming of High-Order Harmonics Generated from Laser-Plasma Interactions, Phys. Rev. Lett. **110**, 165002 (2013).
[26] A. Leblanc, S. Monchocé, H. Vincenti, S. Kahaly, J.-L. Vay, and F. Quéré, Spatial Properties of High-Order Harmonic Beams from Plasma Mirrors: A Ptychographic Study, Phys. Rev. Lett. **119**, 155001 (2017).
[27] D. an der Brügge and A. Pukhov, Propagation of relativistic surface harmonics radiation in free space, Phys. Plasmas **14**, 093104 (2007).
[28] L. G. Gouy, *Sur une Propriété Nouvelle des Ondes Lumineuses* (Gauthier-Villars, Paris, 1890).
[29] S. M. Feng and H. G. Winful, Physical origin of the gouy phase shift, Opt. Lett. **26**, 485 (2001).
[30] R. Hörlein, S. G. Rykovanov, B. Dromey, Y. Nomura, D. Adams, M. Geissler, M. Zepf, F. Krausz, and G. D. Tsakiris, Controlling the divergence of high harmonics from solid targets: A route toward coherent harmonic focusing, Eur. Phys. J. D **55**, 475 (2009).
[31] D. Marcuse, *Light Transmission Optics* (Van Nostrand Reinhold, New York, 1982).
[32] H. Vincenti, Achieving Extreme Light Intensities Using Optically Curved Relativistic Plasma Mirrors, Phys. Rev. Lett. **123**, 105001 (2019).
[33] C. Thaury and F. Quéré, High-order harmonic and attosecond pulse generation on plasma mirrors: Basic mechanisms, J. Phys. B-At. Mol. Opt. Phys. **43**, 213001 (2010).
[34] T. D. Arber, K. Bennett, C. S. Brady, A. Lawrence-Douglas, M. G. Ramsay, N. J. Sircombe, P. Gillies, R. G. Evans, H. Schmitz, and A. R. Bell *et al.*, Contemporary particle-in-cell approach to laser-plasma modelling, Plasma Phys. Control. Fusion **57**, 113001 (2015).
[35] A. Taflove and S. Hagness, *Computational Electrodynamics: The Finite-Difference Time-Domain Method*, Artech House antennas and propagation library (Artech House, 2005).
[36] S. G. García, B. G. Olmedo, and R. G. Martín, A time-domain near- to far-field transformation for fdtd in two dimensions, Microwave Opt. Technol. Lett. **27**, 427 (2000).
[37] M. Born and E. Wolf, *Principles of Optics: Electromagnetic Theory of Propagation, Interference and Diffraction of Light* (Elsevier, London, 2013).
[38] B. Dromey, D. Adams, R. Hörlein, Y. Nomura, S. G. Rykovanov, D. C. Carroll, P. S. Foster, S. Kar, K. Markey, and P. McKenna *et al.*, Diffraction-limited performance and focusing of high harmonics from relativistic plasmas, Nat. Phys. **5**, 146 (2009).
[39] O. Jahn, V. E. Leshchenko, P. Tzallas, A. Kassel, M. Kruger, A. Munzer, S. A. Trushin, G. D. Tsakiris, S. Kahaly, D. Kormin, L. Veisz, V. Pervak, F. Krausz, Z. Major, and S. Karsch, Towards intense isolated attosecond pulses from relativistic surface high harmonics, Optica **6**, 280 (2019).
[40] F. Gori, Flattened gaussian beams, Opt. Commun. **107**, 335 (1994).
[41] A. Forbes, *Laser Beam Propagation: Generation and Propagation of Customized Light* (CRC Press, Boca Raton, 2014).
[42] G. Sansone, L. Poletto, and M. Nisoli, High-energy attosecond light sources, Nat. Photonics **5**, 656 (2011).
[43] J. Li, J. Lu, A. Chew, S. Han, J. Li, Y. Wu, H. Wang, S. Ghimire, and Z. Chang, Attosecond science based on high harmonic generation from gases and solids, Nat. Commun. **11**, 2748 (2020).
[44] L. Gallmann, C. Cirelli, and U. Keller, Attosecond science: Recent highlights and future trends, Annu. Rev. Phys. Chem. **63**, 447 (2012).
[45] M. Uiberacker, T. Uphues, M. Schultze, A. J. Verhoef, V. Yakovlev, M. F. Kling, J. Rauschenberger, N. M. Kabachnik, H. Schröder, and M. Lezius *et al.*, Attosecond real-time observation of electron tunnelling in atoms, Nature **446**, 627 (2007).
[46] S. Cui, P.-L. He, and F. He, Ionization of hydrogen atoms in attosecond pulse trains and strong infrared laser pulses, Phys. Rev. A **94**, 053401 (2016).

[47] T. Fennel, K.-H. Meiwes-Broer, J. Tiggesbäumker, P.-G. Reinhard, P. M. Dinh, and E. Suraud, Laser-driven nonlinear cluster dynamics, Rev. Mod. Phys. **82**, 1793 (2010).

[48] U. Saalmann, I. Georgescu, and J. M. Rost, Tracing nonequilibrium plasma dynamics on the attosecond timescale in small clusters, New J. Phys. **10**, 025014 (2008).

[49] M. T. Hassan, T. T. Luu, A. Moulet, O. Raskazovskaya, P. Zhokhov, M. Garg, N. Karpowicz, A. M. Zheltikov, V. Pervak, F. Krausz, and E. Goulielmakis, Optical attosecond pulses and tracking the nonlinear response of bound electrons, Nature **530**, 66 (2016).

[50] W.-C. Jiang, X.-M. Tong, R. Pazourek, S. Nagele, and J. Burgdörfer, Theory of bound-state coherences generated and probed by optical attosecond pulses, Phys. Rev. A **101**, 053435 (2020).

[51] F. Reiter, U. Graf, E. E. Serebryannikov, W. Schweinberger, M. Fiess, M. Schultze, A. M. Azzeer, R. Kienberger, F. Krausz, A. M. Zheltikov, and E. Goulielmakis, Route to Attosecond Nonlinear Spectroscopy, Phys. Rev. Lett. **105**, 243902 (2010).

[52] S. Chen, C. Ruiz, and A. Becker, Double ionization of helium by intense near-infrared and vuv laser pulses, Phys. Rev. A **82**, 033426 (2010).

[53] M. Nest, F. Remacle, and R. D. Levine, Pump and probe ultrafast electron dynamics in lih: A computational study, New J. Phys. **10**, 025019 (2008).

[54] J. Henkel, T. Witting, D. Fabris, M. Lein, P. L. Knight, J. W. G. Tisch, and J. P. Marangos, Prediction of attosecond light pulses in the vuv range in a high-order-harmonic-generation regime, Phys. Rev. A **87**, 043818 (2013).